Bhatnagar-Gross-Krook subgrid model for neutrino quantum kinetics

Hiroki Nagakura*
Division of Science, National Astronomical Observatory of Japan, 2-21-1 Osawa, Mitaka, Tokyo 181-8588, Japan

Lucas Johns
Theoretical Division, Los Alamos National Laboratory, Los Alamos, New Mexico 87545, USA

Masamichi Zaizen
Faculty of Science and Engineering, Waseda University, Tokyo 169-8555, Japan

(Received 29 December 2023; accepted 15 March 2024; published 9 April 2024)

We present a new subgrid model for neutrino quantum kinetics, which is primarily designed to incorporate effects of collective neutrino oscillations into neutrino-radiation-hydrodynamic simulations for core-collapse supernovae and mergers of compact objects. We approximate the neutrino oscillation term in a quantum kinetic equation using the Bhatnagar-Gross-Krook (BGK) relaxation-time prescription, and the transport equation is directly applicable for classical neutrino transport schemes. The BGK model is motivated by recent theoretical indications that nonlinear phases of collective neutrino oscillations settle into quasisteady structures. We explicitly provide basic equations of the BGK subgrid model for both multiangle and moment-based neutrino transport to facilitate the implementation of the subgrid model in the existing neutrino transport schemes. We also show the capability of our BGK subgrid model by comparing it to fully quantum kinetic simulations for fast neutrino-flavor conversion. We find that the overall properties can be well reproduced in the subgrid model; the error of angular-averaged survival probability of neutrinos is within ∼20%. By identifying the source of error, we also discuss perspectives to improve the accuracy of the subgrid model.

DOI: 10.1103/PhysRevD.109.083013

I. INTRODUCTION

Astrophysical phenomena usually involve intricately intertwined multiphysics. Direct numerical simulation is an effective tool to study the physical mechanism behind these complex phenomena, and also to provide theoretical models for interpretations of the observed data. Often, however, the temporal and spatial scales among different physical processes span many orders of magnitudes, rendering the first-principles simulations prohibitively computationally expensive. This indicates the need for approximations or coarse-grained approaches.

It has been recognized for many years that neutrino quantum kinetics in core-collapse supernovae (CCSNe) and mergers of compact objects represented by a binary neutron star merger (BNSM) corresponds to such a problem requiring coarse-grained treatments (see the reviews in [1–5]). Neutrino-flavor conversion is a representative quantum feature, and various types of neutrino-flavor conversions associated with neutrino self-interactions occur in CCSNe [6–8] and BNSMs [9,10]. On the other hand, the length scale of flavor conversions is much smaller than the astrophysical size, making the first-principles simulations intractable. Although neutrino-radiation-hydrodynamic simulations have matured significantly, one should keep in mind that large uncertainties still remain concerning the impacts of neutrino-flavor conversions even in the current state-of-the-art numerical simulations. Since neutrino-matter interactions depend on neutrino flavors, flavor conversions change the feedback to the fluid dynamics [11–13] and also nucleosynthesis [14–19]. We also note that the dynamics of flavor conversion and its asymptotic behavior hinge on the global advection of neutrinos [11,20–23], exhibiting that global neutrino-radiation-hydrodynamic simulations that incorporate effects of flavor conversions are mandatory for studying the astrophysical consequences of flavor conversions.

There is respectable previous work that incorporates effects of neutrino-flavor conversion in global neutrino-radiation-hydrodynamic simulations in CCSNe and BNSMs [12,13,16–18]. Although the details vary, a neutrino-mixing prescription is commonly added to classical neutrino transport schemes, in which researchers shuffle neutrino flavors one way or another. It should be noted that all mixing

*hiroki.nagakura@nao.ac.jp

 © 2024 American Physical Society

schemes employ rather phenomenological treatments, and hence these results need to be considered provisional. This is mainly because the current implementation of flavor conversion in their codes are rather schematic, which does not allow robust conclusions to be drawn about impacts of flavor conversions. Improving their neutrino mixing schemes is obviously needed, but it is very difficult with the proposed approaches. More importantly, it is not clear how we can give feedback from the results of fully quantum kinetic neutrinos to these phenomenological models. This paper is meant to address this issue and to provide a new way to fill the gap between phenomenological and first-principles simulations.

In this paper, we propose another coarse-grained neutrino transport approach: subgrid-scale modeling for neutrino-flavor conversions. We distinguish our method from other phenomenological approaches since the method is designed to reproduce the spatially and time-averaged features of neutrino-flavor conversions obtained from quantum kinetic neutrino simulations. The noticeable advantage of our subgrid model is having a refinable formulation for dynamics of flavor conversions in various ways, including analytical methods [24–27] and artificial intelligence (AI) techniques [28]. In this paper, we also demonstrate classical neutrino transport simulations with the subgrid model in which we employ a simple but physically motivated subgrid model for flavor conversions.

This paper is organized as follows. In Sec. II, we start by explaining the philosophy of our proposed method. We then provide the quantum kinetic equation with our subgrid model. We also provide its two-moment formalism in Sec. III. These transport equations are written in terms of the $3+1$ general relativistic formulation, which would be helpful for those who work on CCSN and BNSM simulations. After we discuss some details of the method in Sec. IV, we highlight novelties of our subgrid model by comparing it to other phenomenological approaches in Sec. V. In Sec. VI, we discuss the relevance to another coarse-grained approach: miscidynamics [29]. As shown in the section, this formulation is closely associated with our formulation, indicating that the two approaches are complementary. To show the capability of our subgrid model, we demonstrate numerical simulations by using both quantum kinetic neutrino transport and classical transport with the subgrid model, paying attention to fast neutrino-flavor conversion (FFC) in Sec. VII. By comparing their results, we can learn the source of errors in the subgrid model. We then discuss strategies on how to improve them based on studies of quantum kinetic neutrino transport. Finally, we summarize our work in Sec. VIII. Unless otherwise stated, we work with the units $c=\hbar=1$, where c and $\hbar$ are the speed of light and the reduced Planck constant, respectively. In this paper, we will describe all equations with the metric signature $-+++$.

II. BASIC EQUATION FOR NEUTRINO TRANSPORT WITH BHATNAGAR-GROSS-KROOK SUBGRID MODELING

It has been discussed that neutrino-flavor conversions have quasisteady and asymptotic behavior in the nonlinear phase [25–27,30–34] or quasiperiodic properties represented as pendulum motions in flavor space [35–41]. We are interested in the time- and spatially averaged states in the late nonlinear phase since it is unlikely that fine structures with short-time or small-length variations affect astrophysical consequences. Motivated by these studies, we assume that flavor conversions make the radiation field settle into an asymptotic state, and the asymptotic density matrix of neutrinos is denoted by f^a.

In general, the nonlinear evolution of flavor conversions is very complex, and details hinge on flavor instabilities, neutrino-matter interactions, and global geometries of radiation fields. On the other hand, there is always a characteristic timescale of flavor conversions or associated flavor instabilities, which is denoted by τ_a in the following discussion. We note that the timescale depends on the neutrino energy, the angle, and the neutrino flavor. τ_a also provides a rough estimation of the timescale over which the density matrix of the neutrinos settles into f^a.

The quantum kinetic equation (QKE) for neutrino transport can be written as

$$p^\mu \frac{\partial f}{\partial x^\mu} + \frac{dp^i}{d\tau}\frac{\partial f}{\partial p^i} = -p^\mu u_\mu S + i p^\mu n_\mu [H, f], \qquad (1)$$

where f denotes the density matrix of the neutrinos. In the expression, p^μ, x^μ, and τ denote the neutrino four-momentum, the spacetime coordinates, and the affine parameter for the trajectories of the neutrinos, respectively. u^μ, n^ν, S, and H on the right-hand side of Eq. (1) represent the four-velocity of the fluid, the unit vector normal to the spatial hypersurface in four-dimensional spacetimes, the collision term, and the neutrino oscillation Hamiltonian, respectively. Below, we approximate Eq. (1) by using f^a and τ_a.

Our subgrid model is developed based on an assumption that the neutrino distributions are relaxed to f^a via flavor conversions in the timescale of τ_a. This corresponds to a relaxation-time approximation proposed by Bhatnagar-Gross-Krook (BGK) [42], who used the approximation of the collision term in the Boltzmann equation for gas dynamics. In our BGK subgrid model, we apply the model to the neutrino oscillation Hamiltonian [the second term on the right-hand side of Eq. (1)],

$$p^\mu \frac{\partial f}{\partial x^\mu} + \frac{dp^i}{d\tau}\frac{\partial f}{\partial p^i} = -p^\mu u_\mu S + p^\mu n_\mu \frac{1}{\tau_a}(f - f^a). \qquad (2)$$

We note that the relaxation time (τ_a) is measured in the laboratory (or n) frame, but it can be changed based on the

fluid rest frame (see also [43]), which may be useful for the frequently used two-moment formalism for neutrino transport (see Sec. III). It should also be noted that f^a and τ_a are determined from f at each time step, implying that they are time-dependent quantities.

It should be mentioned that the BGK subgrid model (or relaxation-time approximation) is applicable to any system for which there is an equilibrium (or asymptotic) state. As shown in [44], neutrino-flavor conversion is ergodic (at least approximately), thus indicating that the dynamical feature is similar to thermodynamics. The equilibration occurs because it is the most probable (entropy-maximizing) outcome (see also [29]).

It is worth noting that a similar approximation was used to obtain a temporally coarse-grained quantum kinetic equation for the production of sterile neutrinos [see Eqs. (4) and (5) of [45]]. There it was proposed that the entire right-hand side, including both oscillation and collision terms, should be treated using a BGK approximation. This ansatz showed excellent agreement with the numerical results. Here we adapt the relaxation-time approximation to the context of collective neutrino oscillations by proposing that it can be applied to oscillations alone, with subgrid relaxation being caused by collective modes rather than collisions.

From a practical point of view, we also provide a conservative form of Eq. (2), which is used for numerical simulations for both Boltzmann and quantum kinetic neutrino transport (see, e.g., [43,46]). Following [47], we can rewrite the transport equation as

$$\begin{aligned}&\frac{1}{\sqrt{-g}}\frac{\partial}{\partial x^\alpha}\bigg|_{q_i}\left[\left(n^\alpha+\sum_{i=1}^{3}\ell_{(i)}e^\alpha_{(i)}\right)\sqrt{-g}f\right]\\&-\frac{1}{\varepsilon^2}\frac{\partial}{\partial\varepsilon}(\varepsilon^3 f\omega_{(0)})+\frac{1}{\sin\theta_\nu}\frac{\partial}{\partial\theta_\nu}(\sin\theta_\nu f\omega_{(\theta_\nu)})\\&+\frac{1}{\sin^2\theta_\nu}\frac{\partial}{\partial\phi_\nu}(f\omega_{(\phi_\nu)})=DS-\frac{1}{\tau_a}(f-f^a).\end{aligned}\tag{3}$$

In the expression, ε and g are the neutrino energy measured from an $e^\alpha_{(0)}=n^\alpha$ observer, i.e., $\varepsilon\equiv-p_\alpha n^\alpha$ and the determinant of the four-dimensional metric, respectively. $e^\alpha_{(i)}$ $(i=1,2,3)$ denotes a set of the (spatial) tetrad bases normal to n. θ_ν and ϕ_ν denote the neutrino flight direction in the laboratory (or n) frame. These angles are measured from $e^\alpha_{(1)}$, and the three coefficients of ℓ_i represent the directional cosines, which can be expressed as

$$\begin{aligned}\ell_{(1)}&=\cos\theta_\nu,\\\ell_{(2)}&=\sin\theta_\nu\cos\phi_\nu,\\\ell_{(3)}&=\sin\theta_\nu\sin\phi_\nu.\end{aligned}\tag{4}$$

D on the right-hand side of Eq. (3) represents the effective Doppler factor, which is defined as $D\equiv\nu/\varepsilon$ with $\nu\equiv-p^\mu u_\mu$, while ν denotes the neutrino energy measured in the fluid rest frame. $\omega_{(0)},\omega_{(\theta_\nu)},\omega_{(\phi_\nu)}$ on the left-hand side of Eq. (3) can be written as

$$\begin{aligned}\omega_{(0)}&\equiv\varepsilon^{-2}p^\alpha p_\beta\nabla_\alpha n^\beta,\\\omega_{(\theta_\nu)}&\equiv\sum_{i=1}^{3}\omega_i\frac{\partial\ell_{(i)}}{\partial\theta_\nu},\\\omega_{(\phi_\nu)}&\equiv\sum_{i=2}^{3}\omega_i\frac{\partial\ell_{(i)}}{\partial\phi_\nu},\\\omega_i&\equiv\varepsilon^{-2}p^\alpha p_\beta\nabla_\alpha e^\beta_{(i)}.\end{aligned}\tag{5}$$

Spherical polar coordinate is often employed in multiangle neutrino transport codes (see, e.g., [43,48,49]). We hence choose a set of tetrad bases $e_{(i)}$ as

$$\begin{aligned}e^\alpha_{(1)}&=(0,\gamma_{rr}^{-1/2},0,0),\\e^\alpha_{(2)}&=\left(0,-\frac{\gamma_{r\theta}^{-1/2}}{\sqrt{\gamma_{rr}(\gamma_{rr}\gamma_{\theta\theta}-\gamma_{r\theta}^2)}},\sqrt{\frac{\gamma_{rr}}{\gamma_{rr}\gamma_{\theta\theta}-\gamma_{r\theta}^2}},0\right),\\e^\alpha_{(3)}&=\left(0,\frac{\gamma^{r\phi}}{\sqrt{\gamma^{\phi\phi}}},\frac{\gamma^{\theta\phi}}{\sqrt{\gamma^{\phi\phi}}},\sqrt{\gamma^{\phi\phi}}\right),\end{aligned}\tag{6}$$

where $\gamma^{\alpha\beta}\equiv g^{\alpha\beta}+n^\alpha n^\beta$.

One thing we do notice here is that Eq. (2) [or Eq. (3)] corresponds to a classical transport equation if we neglect the off-diagonal elements. Since the main purpose of this study is to provide a subgrid model of neutrino-flavor conversion for classical neutrino transport schemes, we limit our discussion to classical transport with the BGK subgrid model. One should keep in mind that the subgrid model can be applied to neutrino quantum kinetics, and appropriate modeling of off-diagonal components would increase the physical fidelity of the subgrid model. This is an intriguing possibility that deserves further investigation, although we postpone the study to future work.

Below, let us consider how to determine diagonal components of f^a. It is well known that the lepton number of neutrinos/antineutrinos does not change during flavor conversions. This indicates that we can characterize f^a via the survival probability of neutrinos (η), while it depends on neutrino energy and flight angle in general. Following the prescriptions in [24,50–52], we can write f^a in terms of f as

$$\begin{aligned}f^a_e&=\eta f_e+(1-\eta)f_x,\\f^a_x&=\frac{1}{2}(1-\eta)f_e+\frac{1}{2}(1+\eta)f_x,\end{aligned}\tag{7}$$

where f_e and f_x represent distribution functions (or diagonal elements of density matrix) for electron-type and heavy-leptonic-type neutrinos, respectively. We note

that μ and τ neutrinos are assumed to be the same in Eq. (7), which is a reasonable assumption for CCSNe and BNSMs. However, they are quantitatively different from each other, particularly for high energy neutrinos (see, e.g., [53]), due to high-order corrections in neutrino-matter interactions (e.g., weak magnetism [54]). We also note that if on-shell muons appear [55–57], we should distinguish between the μ and τ neutrinos. We can deal with these cases by introducing another parameter to represent neutrino mixing. For antineutrinos, we can use the same form as in Eq. (7) but replace f and η with $\bar{f}$ and $\bar{\eta}$, respectively.

There are two important remarks about our BGK subgrid model. First, f^a (or η) hinges on flavor instabilities, and it should be determined (or calibrated) based on neutrino quantum kinetics. It is important to note that the results from analytic studies and local simulations of flavor conversions can be directly used to determine it. In Sec. VII, we demonstrate such simulations for FFC. Second, if the system contains multiple flavor instabilities, we can handle the problem with multiple BGK terms. More specifically, the second term on the right-hand side of Eq. (2) can be rewritten as

$$p^\mu n_\mu \frac{1}{\tau_a}(f - f^a) \to p^\mu n_\mu \sum_{i=1}^{N} \frac{1}{\tau_{a_i}}(f - f^{a_i}), \tag{8}$$

where the index i distinguishes the flavor instabilities among N modes. As shown in Eq. (8), the contribution of each term is characterized by τ_{a_i} and $f - f^{a_i}$, which guarantees that flavor conversion with a shorter relaxation time and a large difference between f and f^{a_i} dominates the system. This prescription may be important for realistic CCSN and BNSM models since FFC and collisional flavor instabilities (CFIs) may occur simultaneously (see, e.g., [8]) at the same position. The extension in Eq. (8) allows us to study the situation where multiple flavor instabilities are competing to each other.

Before we discuss how to estimate τ_a in Sec. IV, let us describe the two-moment transport formalism for our subgrid model in the next section. This is helpful for those who use the moment formalism for numerical modeling of CCSNe and BNSMs.

III. TWO-MOMENT FORMALISM

Moment formalism of radiation transport has, in principle, the ability to describe full neutrino kinetics with equivalent levels of Boltzmann (or fully quantum kinetic) neutrino transport. In practice, however, the moment formalism results in an infinite hierarchy of coupled equations, indicating that we need to truncate the hierarchy of moments at a certain rank. The most popular current approach in neutrino transport simulations is two-moment formalism [58–69], in which the zeroth and first angular moments correspond to fundamental variables. We determine their time evolution and spatial distributions by solving their coupling equations, while higher-rank moments are complemented by closure relations. It is worth noting that the moment formalism is also used for the study of neutrino-flavor conversions [36,70–73]. In this section, we provide an explicit description of the two-moment formalism in the BGK subgrid model.

Following the convention of [58], we decompose the neutrino four-momentum (p^α) into u^α and its orthogonal normal vector (ℓ^α) as

$$p^\alpha = \nu(u^\alpha + \ell^\alpha), \tag{9}$$

where the conditions of $\ell^\alpha u_\alpha = 0$ and $\ell^\alpha \ell_\alpha = 1$ are satisfied. The unprojected second- and third-rank moments of neutrinos are defined as (see also [74])

$$\begin{aligned} M^{\alpha\beta} &\equiv \nu^3 \int f(u^\alpha + \ell^\alpha)(u^\beta + \ell^\beta) d\Omega, \\ M^{\alpha\beta\gamma} &\equiv \nu^3 \int f(u^\alpha + \ell^\alpha)(u^\beta + \ell^\beta)(u^\gamma + \ell^\gamma) d\Omega, \end{aligned} \tag{10}$$

where Ω denotes the solid angle of neutrino momentum space defined in the fluid rest frame. It should be mentioned that the integral of $M^{\alpha\beta}$ over the neutrino energy ($\int M^{\alpha\beta} d\nu$) corresponds to the energy-momentum tensor of the neutrinos. We also define the zeroth and first angular moments defined in the fluid rest frame as

$$\begin{aligned} J &\equiv \nu^3 \int f d\Omega, \\ H^\alpha &\equiv \nu^3 \int \ell^\alpha f d\Omega, \\ L^{\alpha\beta} &\equiv \nu^3 \int \ell^\alpha \ell^\beta f d\Omega, \\ N^{\alpha\beta\gamma} &\equiv \nu^3 \int \ell^\alpha \ell^\beta \ell^\gamma f d\Omega. \end{aligned} \tag{11}$$

Using these variables, the basic equation for the two-moment formalism with BGK subgrid model can be written as [see also Eq. (2)]

$$\nabla_\beta M^{\alpha\beta} - \frac{\partial}{\partial \nu}(\nu M^{\alpha\beta\gamma} \nabla_\gamma u_\beta) = S^\alpha - W^\alpha, \tag{12}$$

where

$$\begin{aligned} S^\alpha &\equiv \nu^3 \int S(u^\alpha + \ell^\alpha) d\Omega, \\ W^\alpha &\equiv \frac{1}{\tau_a^{\rm fl}} \nu^3 \int (f - f^a)(u^\alpha + \ell^\alpha) d\Omega, \end{aligned} \tag{13}$$

where $\tau_a^{\rm fl} \equiv D\tau_a$. Equation (12) indicates that the BGK subgrid model can be implemented simply by replacing

$S^\alpha \to S^\alpha - W^\alpha$ from the original two-moment formalism. W^α can be expressed in a form similar to the emission-absorption process of the collision term, which can be written as

$$W^\alpha = \frac{1}{\tau_a^{\rm fl}}((J - J^a)u^\alpha + (H^\alpha - H^{\alpha a})). \tag{14}$$

We hence need to determine τ_a, J^a, and $H^{\alpha a}$ to implement the BGK model.

J^a and $H^{\alpha a}$ can be obtained by taking the angular integrals of Eq. (7), and it looks as though the process is straightforward. However, η depends on Ω in general, indicating that we need higher-rank angular moments to evaluate them. Below, we provide an approximate prescription to address this issue.

We start by expanding the angular dependence of η by ℓ_α as

$$\eta = \eta_0 + \eta_1^\alpha \ell_\alpha + \eta_2^{\alpha\beta}\ell_\alpha\ell_\beta + \cdots, \tag{15}$$

where the coefficients (η_i) do not depend on Ω. Using the expression, J^a and $H^{\alpha a}$ can be written as

$$\begin{aligned}
J_e^a &= J_x + \eta_0(J_e - J_x) + \eta_1^\alpha(H_{e\alpha} - H_{x\alpha}) + \eta_2^{\alpha\beta}(L_{e\alpha\beta} - L_{x\alpha\beta}) + \cdots \\
H_e^{\alpha a} &= H_x^\alpha + \eta_0(H_e^\alpha - H_x^\alpha) + \eta_1^\beta(L_{e\beta}^\alpha - L_{x\beta}^\alpha) + \eta_2^{\beta\gamma}(N_{e\beta\gamma}^\alpha - N_{x\beta\gamma}^\alpha) + \cdots \\
J_x^a &= \frac{1}{2}(J_e + J_x) - \frac{\eta_0}{2}(J_e - J_x) - \frac{\eta_1^\alpha}{2}(H_{e\alpha} - H_{x\alpha}) - \frac{\eta_2^{\alpha\beta}}{2}(L_{e\alpha\beta} - L_{x\alpha\beta}) + \cdots \\
H_x^{\alpha a} &= \frac{1}{2}(H_e^\alpha + H_x^\alpha) - \frac{\eta_0}{2}(H_e^\alpha - H_x^\alpha) - \frac{\eta_1^\beta}{2}(L_{e\beta}^\alpha - L_{x\beta}^\alpha) - \frac{\eta_2^{\beta\gamma}}{2}(N_{e\beta\gamma}^\alpha - N_{x\beta\gamma}^\alpha) + \cdots.
\end{aligned} \tag{16}$$

This method guarantees that flavor-integrated angular moments are conserved, regardless of η_i, even if we truncate their angular moments at any order.

Equation (16) exhibits that the accuracy of determining J^a and $H^{\alpha a}$ hinges on how well we can determine the coefficients η_i. In two-moment neutrino transport code, the maximum-entropy completion [75,76] (or the fitting method proposed in [77], which can be used only for CCSNe, though) may be useful to obtain physically reasonable solutions. A noticeable feature of these methods is that we approximately reconstruct full angular distributions of neutrinos from their zeroth and first angular moments. This suggests that the angular dependence of η can be determined in a similar way as multiangle neutrino transport (see Sec. VII B for more details).

Neglecting energy dependence and anisotropic components in η, i.e., $\eta(\nu, \Omega) = \eta_0$, corresponds to the simplest case, but it would be a reasonable approximation of CFI. Since the CFI becomes important in regions where neutrinos and matters are tightly coupled, neutrinos are nearly isotropic in momentum space [8,78]. We also note that the so-called isotropy-preserving branch in $k = 0$ mode provides the maximum growth rate of the instability [79], thereby leading to confidence about diminishing the angular dependence in η. Regarding the energy dependence, on the other hand, Liu *et al.* [79] found that the growth rate of CFI can be well approximated by the monochromatic energy treatment with averaged-energy collision rates. We also note that flavor swap is accompanied by resonancelike CFI, but the dynamics does not depend on neutrino energy [80], suggesting that energy dependence is not important in these cases.

The condition $\eta(\nu, \Omega) = \eta_0$ corresponds to the simplest case for our BGK model, but it would be useful to explore qualitative trends for impacts of flavor conversions on CCSNe and BNSM, as studied with phenomenological approaches. It should be emphasized that our subgrid model takes into account the relaxation timescale, indicating that the interaction between neutrino advection, neutrino-matter interaction, and flavor conversions would be more appropriately handled than other phenomenological ones. It seems that $\eta_0 = 1/3$ and 0 are two interesting cases which correspond to flavor equipartition and flavor swap, respectively.

IV. ESTIMATION FOR τ_a

The vigor of flavor conversion cannot be measured only by f^a. Even if the asymptotic distribution is very different from the original nonmixing state, the flavor conversion cannot be completed if the relaxation time is very long. This exhibits that the determination of τ_a is also an important task for increasing the accuracy of our subgrid model.

Linear stability analysis can offer the growth rate of flavor conversion, which would be the most accurate determination of τ_a. However, the growth rate can be obtained by solving the dispersion relation (see, e.g., [81,82]), which is a computationally expensive task. We also note that, in the stability analysis, full energy- and angular-dependent information regarding neutrinos in momentum space is required

in general, but it can be obtained only by solving multiangle and multienergy neutrino transport, indicating that this information is not available for approximate neutrino transport. We hence need alternative approaches for the estimation of τ_a to suit our needs.

We can utilize some approximate approaches to stability analysis that have been proposed in the literature. For FFC, a simple formula was provided in [83,84]. In this method, we can approximately estimate τ_a as

$$\tau_a \sim 2\pi \left| \left(\int_{G_v>0} d\Gamma G_v \right) \left(\int_{G_v<0} d\Gamma G_v \right) \right|^{-1/2}, \quad (17)$$

where

$$d\Gamma_v \equiv \frac{1}{4\pi} d(\cos\theta_\nu) d\phi_\nu,$$
$$G_v \equiv \frac{1}{2\pi^2} \int ((f_e - \bar{f}_e) - (f_x - \bar{f}_x)) \varepsilon^2 d\varepsilon. \quad (18)$$

In Sec. VII, we demonstrate neutrino transport simulations for FFC by using Eq. (18).

It is also noteworthy that Eq. (17) is applicable to the two-moment method using maximum-entropy completion [75,76] or a fitting method [77] since either can approximately retrieve f from the zeroth and first angular moments. It would also be useful to employ other methods, as in [73,75,76,79,85–87], which allow us to evaluate the growth rate of flavor conversions directly from low angular moments of neutrinos. For CFI, the growth rate can also be estimated analytically [10,79,88], which is useful in our subgrid model. We can select them depending on the problem and the purpose of study. Another remark here is that machine-learning techniques potentially provide accurate estimations of η and τ_a without a significant computational burden (see, e.g., [28,89,90]).

V. COMPARISONS WITH OTHER PHENOMENOLOGICAL MODELS

It would be worthwhile to highlight differences of our subgrid model from other phenomenological methods implemented in some neutrino-radiation-hydrodynamic codes. The study by [16] corresponds to a pioneer work for BNSM simulations with a phenomenological model of FFC, in which the effects of FFC are incorporated via a parametric prescription. In their method, occurrences of FFC are identified based on $k = 0$ mode stability analysis. They shuffle neutrinos among ν_e, ν_μ, and ν_τ to have flavor equipartition if the timescale of flavor conversion is shorter than the critical one (which was assumed to be 10^{-7} s). This indicates that their prescription of flavor conversion can be reproduced in our subgrid model by setting $\eta = 1/3$ and $\tau_a \to 0$ if the growth timescale is shorter than 10^{-7} s (otherwise, τ_a is set to infinity).

In [18], Just *et al.* carried out BNSM simulations using an approach similar to that in [16], but they studied impacts of FFCs on BNSM dynamics by considering three types of neutrino mixing schemes. Essentially, the degree of neutrino mixing varies among schemes, while the detection criterion for occurrences of FFC is common, in which they determine FFCs only by energy-averaged flux factor of $\bar{\nu}_e$. They also assumed that flavor conversions occur instantaneously (e.g., $\tau_a \to 0$ in our BGK subgrid model). This approach can also be reproduced using our subgrid model.

A similar study for FFCs in BNSM has also been made by [17]. Unlike [16,18], Fernández *et al.* employed a so-called leakage scheme for neutrino transport. In their method, the neutrino transport scheme is left as the original, but they changed the estimation of neutrino luminosity by taking into account FFCs, which corresponds to a key ingredient in their scheme to give a feedback of neutrinos to fluid dynamics and ejecta compositions. They determine asymptotic neutrino luminosities by varying parameters (including cases with flavor equipartition), while they also employ neutrino opacities to determine the degree of mixing. In their approach, flavor conversions are suppressed in an optically thick region, whereas they occur in an optically thin one. Since this phenomenological model is developed based on a different philosophy than ours, our subgrid model cannot reproduce their model. Nevertheless, it is interesting to compare our subgrid model to their phenomenological model in CCSN and BNSM simulations.

The impacts of FFC on CCSN dynamics have been studied with another phenomenological approach in [12,13]. In the method of Ehring *et al.*, there are three independent neutrino flavors, ν_e, $\bar{\nu}_e$, and ν_x, which they shuffle so as to guarantee the neutrino lepton number conversion. They employ matter density to determine occurrences of FFC, in which there is a threshold density that flavor conversions occur. In the region where the matter density is lower than the threshold, they assume that neutrino-flavor conversions occur instantaneously. They also assume that neutrinos are in flavor equilibrium, but ν_x and $\bar{\nu}_x$ are assumed to be identical after the conversion is completed. As such, this phenomenological model is developed based on a very different approach from our subgrid one.

One of the interesting applications for our subgrid model is to assess the capability of each phenomenological model. The assessment has been impossible thus far through direct numerical simulations of quantum kinetic neutrino transport due to extremely high computational cost, but it is feasible using our subgrid model. This study would also help us to improve each phenomenological model.

VI. COMPARISON WITH MISCIDYNAMICS

The coarse-grained subgrid model is compatible with the proposal to approximate neutrino quantum kinetics using neutrino quantum thermodynamics [29]. Taking $\tau_a \to 0$ in Eq. (2) results in

$$p^\mu \frac{\partial f^a}{\partial x^\mu} + \frac{dp^i}{d\tau}\frac{\partial f^a}{\partial p^i} = -p^\mu u_\mu S^a, \tag{19}$$

where S^a is S evaluated using $f = f^a$. This equation is equivalent to the miscidynamic transport equation written in Ref. [29] if f^a is equated to $\rho^{\rm eq}$ in that paper.

Miscidynamics refers to coarse-grained neutrino transport based on the concept of local mixing equilibrium. Our subgrid model does not necessarily assume that f^a is an equilibrium state in a thermodynamic sense. If we do assume this, however, then taking the limit of short relaxation time τ_a is a means of imposing local mixing equilibrium. The thermodynamic input then enters through the determination of f^a.

If $\tau_a \to 0$, the neutrino flavor instantaneously equilibrates; therefore, it should never depart from equilibrium in the first place. This is the idea behind the adiabatic proposal of Ref. [29]. Accepting this logic, it is then possible to determine f^a using the assumption of adiabaticity and the requirements of self-consistency. Adiabaticity relates f to the Hamiltonian, but the Hamiltonian is itself a function of f through neutrino-neutrino forward scattering—hence the need for self-consistency. In the more straightforward case of Mikheyev-Smirnov-Wolfenstein flavor conversion without neutrino self-interactions, self-consistency is not required and f^a is determined simply by vacuum oscillations and neutrino-matter forward scattering.

Finite equilibration rates entail some amount of entropy production. Formulating diabatic miscidynamics—in contrast to the adiabatic version described above—would require a consideration of how subgrid degrees of freedom in the neutrino-flavor field respond to grid-level changes driven by the derivative and collisional terms in Eq. (2). Generally speaking, if the microscopic constituents respond very quickly, then the macroscopic system moves between equilibria with minimal entropy production. Equations supplementing miscidynamics with diabatic terms have not yet been worked out. In their absence, the relaxation time τ_a is a simple and plausible approximation of diabaticity.

One subtlety in using our BGK subgrid model for diabatic miscidynamics is that f^a changes under diabatic evolution. The system heats up, and mixing equilibrium is set by the system itself rather than an external environment. Because entropy production is a subgrid effect, f^a can change on a subgrid timescale, which threatens the use of coarse graining. However, a simple approximation is to adopt

$$f^a \longrightarrow f^a_\infty, \qquad \tau_a \longrightarrow \tau^\infty_a, \tag{20}$$

where f^a_∞ and τ^∞_a are the $t \to \infty$ equilibrium and relaxation time. In this approximation, the neutrino flavor relaxes directly toward the ultimate equilibrium state f^a_∞ rather than pursuing a time-evolving equilibrium that converges on f^a_∞ at late times. The form of Eq. (2) is unchanged, except for replacements of f^a and τ_a with the respective asymptotic quantities.

In sum, the $\tau_a \to 0$ relaxation subgrid model can reproduce adiabatic miscidynamics. Miscidynamics can be systematically improved by calculating diabatic corrections from the statistical mechanics underlying neutrino quantum thermodynamics [29]. It appears that Eq. (2) can likewise be systematically improved by adjusting f^a and τ_a to reflect these corrections.

VII. DEMONSTRATION

In this section, we discuss capabilities of our BGK subgrid model by carrying out local simulations of FFC in one spatial dimension. Under the symmetry, neutrino angular distributions in momentum space become axisymmetric, indicating that we solve the QKE for one in time, one in real space, and one in momentum space. We select this problem because analytic schemes for determining asymptotic states of FFC have been proposed in the literature [25,27] which can be used to compute f^a. After we describe essential information on numerical simulations, we explicitly describe how to determine f^a.

A. Full quantum kinetic simulations

Here we describe the problem under a full quantum kinetic approach. Note that the results of these simulations will be used to assess simulations with the BGK subgrid model; details will be given in Sec. VII B. Quantum kinetic simulations in this study are essentially the same as those performed in [24], in which we demonstrated one-dimensional (1D) local simulations of FFCs in a two-flavor framework. One noticeable difference from the previous study is that we solve the QKE under a three-flavor framework. Assuming spherically symmetry and no collision terms, we solve the following QKE:

$$\frac{\partial \overset{(-)}{f}}{\partial t} + \frac{1}{r^2}\frac{\partial}{\partial r}(r^2 \cos\theta_\nu \overset{(-)}{f}) - \frac{1}{r\sin\theta_\nu}\frac{\partial}{\partial \theta_\nu}(\sin^2\theta_\nu \overset{(-)}{f}) = -i[\overset{(-)}{H}, \overset{(-)}{f}], \tag{21}$$

where

$$\overset{(-)}{H} = \overset{(-)}{H}_{\rm vac} + \overset{(-)}{H}_{\rm mat} + \overset{(-)}{H}_{\nu\nu}. \tag{22}$$

In this expression, $f(\bar{f})$ and $H(\bar{H})$ denote the density matrix of the neutrinos and the oscillation Hamiltonian for neutrinos (antineutrinos), respectively. Since we focus only on local simulations in this study, neutrino advection in θ_ν direction is basically negligible. Each term of neutrino Hamiltonian can be written as

$$\bar{H}_{\rm vac} = H^*_{\rm vac},$$
$$\bar{H}_{\rm mat} = -H^*_{\rm mat},$$
$$\bar{H}_{\nu\nu} = -H^*_{\nu\nu}. \tag{23}$$

As in [24], we ignore matter potential in Hamiltonian, but their effects are effectively taken into account in the vacuum potential (see below). The vacuum term, on the other hand, is included in our simulations, which have the following form:

$$H_{\rm vac} = \frac{1}{2\varepsilon} U \begin{bmatrix} m_1^2 & 0 & 0 \\ 0 & m_2^2 & 0 \\ 0 & 0 & m_3^2 \end{bmatrix} U^\dagger, \tag{24}$$

where m_i^2 and U denote the neutrino squared mass for the mass eigenstate of i and the Pontecorvo-Maki-Nakagawa-Sakata matrix, respectively. Neutrino-flavor conversions depend only on the difference of each squared mass of the neutrino, and we set them as $\Delta m_{21}^2 = 7.42 \times 10^{-5}$ eV^2 and $\Delta m_{31}^2 = 2.510 \times 10^{-3}$ eV^2, where $\Delta m_{ij} \equiv m_i^2 - m_j^2$ in this study. We effectively include the effects of matter suppression of flavor conversion by setting the neutrino mixing angles at 10^{-6}, which is much smaller than the constraints imposed by experiments. It should be noted that the vacuum potential is necessary only for triggering flavor conversions, and it does not affect nonlinear evolutions of FFCs. This is simply because the self-interaction potential is several orders of magnitude higher than the vacuum one, which also guarantees that FFCs overwhelm the slow modes. Throughout this test, we use a monochromatic assumption with a neutrino energy of 12 MeV.

In setting up the initial angular distributions of ν_e and $\bar{\nu}_e$, we employ the following analytic formula:

$$\overset{(-)}{f}_{ee} = \langle \overset{(-)}{f}_{ee} \rangle (1 + \overset{(-)}{\beta}_{ee} (\cos\theta_\nu - 0.5)), \quad \cos\theta_\nu \geq 0, \tag{25}$$

where $\langle f_{ee} \rangle$ corresponds to an angular-averaged distribution function for electron-type neutrinos and its bar denotes the same quantity but for antineutrinos. In this model, we vary the angular distributions of neutrinos by changing $\langle \overset{(-)}{f}_{ee} \rangle$ and $\overset{(-)}{\beta}_{ee}$. The former and latter are associated with neutrino number density and asymmetric degree of their angular distributions (see also [20,24]). As in [24], we put a dilute neutrino gas for incoming neutrinos ($\cos\theta_\nu \leq 0$), which do not play a role in FFC. We also assume that there is neither ν_μ nor ν_τ nor any of their antipartners in the initial distributions. Following [24], $\langle f_{ee} \rangle$ is chosen so that the number density of ν_e becomes 10^{32} cm^{-3}. We determine $\langle \bar{f}_{ee} \rangle$ via a new variable, α, which is defined as

$$\alpha \equiv \frac{\langle \bar{f}_{ee} \rangle}{\langle f_{ee} \rangle} = \frac{\bar{n}_{\nu_e}}{n_{\nu_e}}, \tag{26}$$

where n_{ν_e} ($\bar{n}_{\nu_e}$) denotes the number density of ν_e ($\bar{\nu}_e$). In this demonstration, we study four cases by varying α and $\bar{\beta}_{ee}$ while setting $\beta_{ee} = 1$ for all models. The reference model corresponds to the case with $\alpha = 1$ and $\bar{\beta}_{ee} = 1$. We add two models by varying α ($\alpha = 0.9$ and 1.1), while $\bar{\beta}_{ee}$ is the same as the reference one. We test another model with $\bar{\beta}_{ee} = 0.1$, while α is set to be the same as the reference model. It should be mentioned that the angular position for electron-neutrinos lepton number (ELN) crossings hinges on α, and that $\bar{\beta}_{ee}$ dictates the depth of crossing increases (see [24] for more details).

In these simulations, we focus on a spatially narrow region with $50\ {\rm km} \leq r \leq 50\ {\rm km} + 10\ {\rm m}$. The radial domain and angular (θ_ν) direction in neutrino momentum space are covered by $N_r = 49152$ and $N_{\theta_\nu} = 128$ uniform grid points, respectively. We employ a Dirichlet boundary condition for incoming neutrinos from at each boundary position, while the free boundary one is adopted for escaping neutrinos from the computational region. We run each simulation up to 10^{-4} ms.

B. Classical simulations with the BGK subgrid model

The equation in our BGK subgrid model that corresponds to Eq. (21) can be written as

$$\frac{\partial \overset{(-)}{f}}{\partial t} + \frac{1}{r^2}\frac{\partial}{\partial r}(r^2 \cos\theta_\nu \overset{(-)}{f}) - \frac{1}{r\sin\theta_\nu}\frac{\partial}{\partial \theta_\nu}(\sin^2\theta_\nu \overset{(-)}{f})$$
$$= -\frac{1}{\tau_a}(\overset{(-)}{f} - \overset{(-)}{f^a}), \tag{27}$$

while we assume that the off-diagonal terms are zero, implying that Eq. (27) is equivalent to classical neutrino transport. For this simulation, we extend our GRQKNT code [43] by adding the BGK subgrid module. This indicates that these numerical simulations for both full quantum kinetics and this classical Boltzmann transport with the subgrid model have the same accuracy of neutrino advection. The initial and boundary conditions are also the same as those in QKE simulations. In this demonstration, we employ Eq. (17) to estimate τ_a. We note that τ_a is updated at every time step during the simulation.

To determine $\overset{(-)}{f^a}$, we employ a method in [25]. This offers an approximate scheme to determine the asymptotic states of FFC analytically. As we shall discuss later, however, this analytic method corresponds to the simplest prescription, and there is room for improvement. In fact, the scheme is developed based on assumptions that the neutrino flight directions are $v > 0$ (or $v < 0$) and there is a single ELN angular crossing. These assumptions are not appropriate in general, leading to a systematic error in realistic situations.

Nevertheless, this scheme can capture the essential trends of FFCs (see below), which may provide sufficient accuracy as a subgrid model.

In this method, we first compute the positive and negative ELN–heavy-leptonic neutrinos lepton number (XLN) densities,

$$A \equiv \left| \int_{G_v<0} d\Gamma G_v \right|,$$
$$B \equiv \int_{G_v>0} d\Gamma G_v, \tag{28}$$

while G_v is as given in Eq. (18). In cases with $B > A$ (positive ELN-XLN density), we determine η in Eq. (7) as

$$\eta = \begin{cases} \frac{1}{3} & (G_v < 0), \\ 1 - \frac{2A}{3B} & (G_v \geq 0). \end{cases} \tag{29}$$

Meanwhile, η in $B < A$ (negative ELN-XLN density) is determined as

$$\eta = \begin{cases} \frac{1}{3} & (G_v > 0), \\ 1 - \frac{2B}{3A} & (G_v \leq 0). \end{cases} \tag{30}$$

In the case with $B = A$, η is set to be $1/3$ for all v, indicating that f^a corresponds to the complete flavor equipartition (see also [25,27,30]). We also note that $\bar{\eta}$ is equal to η since we do not have to distinguish neutrinos from antineutrinos in FFC (see also [25]).

Let us put an important remark here. As shown in [26], the asymptotic state of FFCs obtained from quantum kinetic simulations depends on boundary conditions. In fact, the Dirichlet boundary condition (as used in this demonstration) results in a qualitatively different asymptotic state than that obtained with the periodic one. In the Dirichlet case, the asymptotic state is determined so as to preserve ELN and XLN fluxes. In this demonstration, however, we determine η from the condition of number conservation [Eqs. (28)–(30)], despite employing the Dirichlet boundary condition. One may wonder whether this is inconsistent treatment. As we shall demonstrate below, however, our choice is appropriate. We will provide this detailed discussion in Sec. VII C.

One of the advantages of the subgrid model is that high resolutions are no longer necessary in these simulations, since there are no driving terms to create small-scale structures in this coarse-grained model. For this reason, we employ $N_r = 192$ and $N_{\theta_\nu} = 16$ grid points with the same domains as those used in QKE simulations. It should be mentioned, on the other hand, that τ_a is much smaller than the advection timescale (which is also associated with the Courant-Friedrich-Lewy condition for the stability of numerical simulations), implying that Eq. (27) becomes a stiff equation. This requires an implicit time evolution to numerically stabilize in solving the equation. In this demonstration, an operator-splitting approach is adopted in which we first evolve f by neutrino advection in time explicitly, and then the BGK term [right-hand side of Eq. (27)] is handled in an implicit way. More specifically, the distribution function of neutrinos at the $n+1$ time step (f^{n+1}) is computed as

$$f^{n+1} = \left(\frac{1}{\Delta t} + \frac{1}{\tau_a}\right)^{-1} \left(\frac{f^*}{\Delta t} + \frac{f^a}{\tau_a}\right), \tag{31}$$

where Δt denotes the time step. In this expression, f^* corresponds to a tentative distribution function which is obtained by f evolved only by advection terms in Eq. (27). We confirm that this operator-splitting method works well to evolve the system in a numerically stable manner.

For the sake of completeness, a resolution study is also undertaken with the reference model ($\alpha = 1$ and $\bar{\beta}_{ee} = 1$) of the subgrid model. One of them is a simulation with twice the spatial resolution of the reference one (i.e., $N_r = 384$), while the angular resolution remains the same. We also carry out another simulation with high angular resolution, $N_{\theta_\nu} = 128$, which corresponds to the same resolution as that adopted in quantum kinetic transport, while the spatial resolution is the same as the reference one ($N_r = 192$). As shown below, these results are essentially the same as the reference model, indicating that simulations employing BGK subgrid models are not sensitive to numerical resolutions.

C. Results

In Fig. 1, we show the color map of survival probability of ν_e as functions of r and $\cos\theta_\nu$. From left to right, results with three different time snapshots are displayed ($T = 10^{-5}, 5 \times 10^{-5}$, and 10^{-4} ms, respectively). The top and bottom panels distinguish the quantum kinetic model from the classical one with the BGK subgrid model. Since antineutrinos have essentially the same properties as those in neutrinos, we omit them.

As shown in the top left panel of Fig. 1, neutrino-flavor conversions vividly occur and nearly reach flavor equipartition in almost the entire neutrino flight directions at $T = 10^{-5}$ ms. This is consistent with previous studies [25,27,30] in that FFC makes the system evolve toward the flavor equipartition in the case with $n_{\nu_e} = n_{\bar{\nu}_e}$. As we discussed in [24,26], however, the flavor equipartition is not the actual asymptotic state in cases with the Dirichlet boundary condition. In fact, angular distributions of survival probability of ν_e become remarkably different around the boundary at $R - R_{\rm in} = 0$; indeed, FFC tends to be less vigorous in $\cos\theta_\nu \gtrsim 0.5$. The region expands with time, and eventually it dominates the entire computational domain (see the middle and right panels in the top row of Fig. 1). We will later discuss in detail the physical mechanism of the transition, which is associated with the determination of f^a from f in BGK subgrid model.

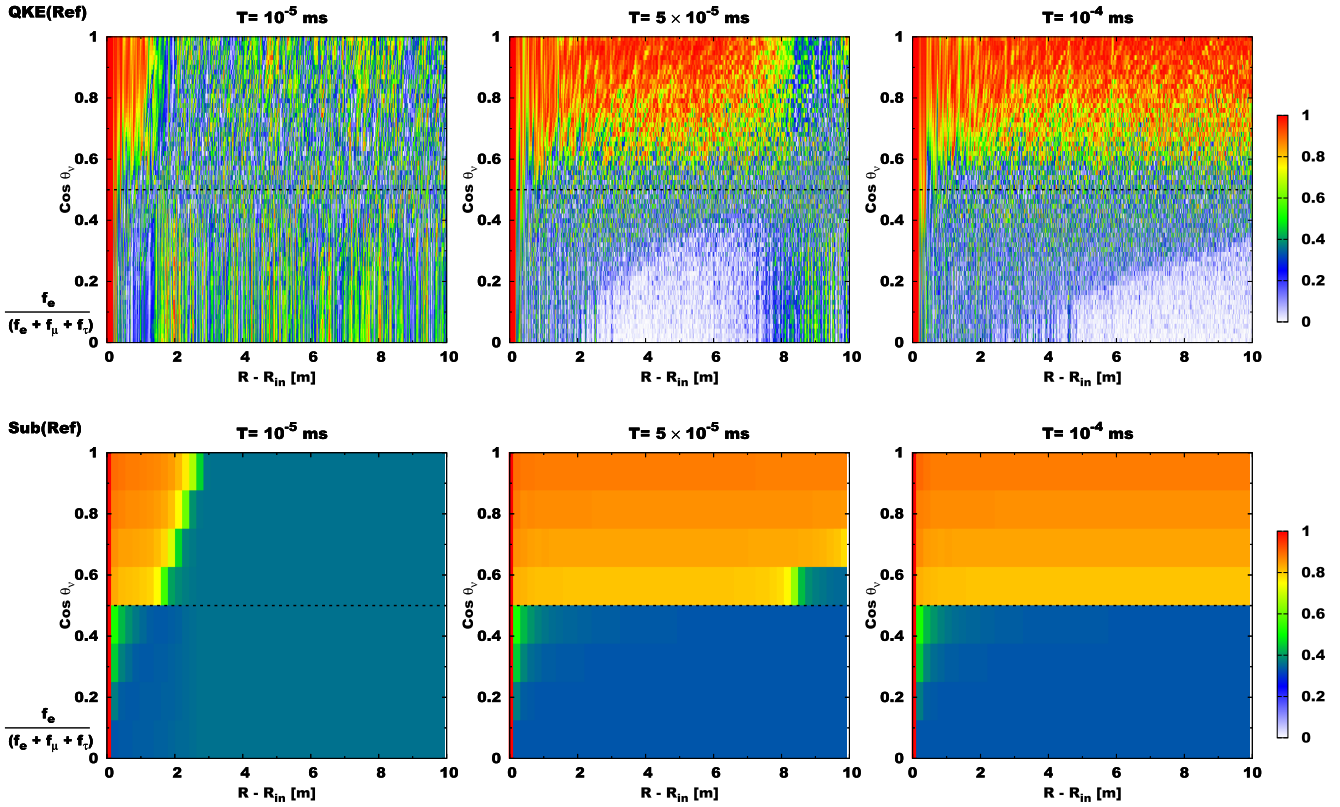

FIG. 1. Color map of survival probability of ν_e for the reference model ($\alpha = 1$ and $\bar{\beta}_{ee} = 1$). The horizontal and vertical axes denote the radius ($R - R_{\rm in}$) and the directional cosine of the neutrino flight angle ($\cos\theta_\nu$), respectively. The dashed line in each panel represents the neutrino angle with an ELN zero crossing at the initial condition. The top and bottom panels distinguish the results of the quantum kinetic simulation from those of the classical one with the BGK subgrid model. From left to right, we show the results at three different time snapshots: $T = 10^{-5}, 5 \times 10^{-5}$, and 10^{-4} ms.

As shown in the bottom panels of Fig. 1, the corresponding classical simulation with the BGK subgrid model can reproduce results that are qualitatively similar to those found in the quantum kinetic simulation. In the earlier phase, FFC occurs in the entire angular regions, except for the vicinity of $R - R_{\rm in} = 0$, but the flavor conversion in $\cos\theta_\nu \gtrsim 0.5$ subsides after neutrinos injected (constant in time) at $R - R_{\rm in} = 0$ reach there. In Fig. 2, we compare the radial profiles of the angular-averaged survival probability of ν_e between the two simulations, and we confirm that the errors are within ∼20%. This comparison leads to confidence in the capability of the BGK subgrid model.

It is interesting to inspect how τ^a and f^a vary in space and evolve with time. To see their essential features, we show the time evolution of τ^a and $n^a_{\nu_e}$ (the number density of electron-type neutrinos computed from f^a_{ee}) at three different radii ($R - R_{\rm in} = 2.5$, 5, and 7.5 m) in Fig. 3. As a reference, we also show n_{ν_e} in the same figure. In the early phase ($T \lesssim 10^{-5}$ ms), τ^a monotonically increases with time, while n_{ν_e} approaches $n^a_{\nu_e}$. These time evolutions are identical for the three different radii, indicating that the system evolves nearly homogeneously. The increase of τ_a indicates that ELN-XLN angular crossings become shallow [see also Eq. (17)] due to $f \to f^a$. At $T \sim 10^{-5}$ ms, the time evolutions of both τ^a and f^a become qualitatively different from that in the earlier phase. This phase corresponds to the transition of asymptotic states from the periodic case to the Dirichlet one. In fact, the onset timing of the phase transition is earlier for a smaller radius, which indicates that the impacts of the Dirichlet boundary condition propagate in the positive radial direction. During the transition phase, both τ^a and $n^a_{\nu_e}$ are dynamically evolved and also inhomogeneous in space; meanwhile, n_{ν_e} keeps approaching $n^a_{\nu_e}$. At $T \sim 10^{-4}$ ms, the system settles into a steady state. Interestingly, τ_a remains finite at different positions, and it varies with the radius even at the end of our simulation. This indicates that ELN-XLN angular crossings do not disappear completely in the steady state, and that ELN-XLN angular crossings are deeper for smaller radii. This trend can be interpreted as the effect of neutrino advection under the Dirichlet boundary condition. Neutrinos having ELN-XLN angular crossings are injected constantly in time at $R = R_{\rm in}$, and the angular crossing fades with the radius. Nevertheless, τ_a is much larger than

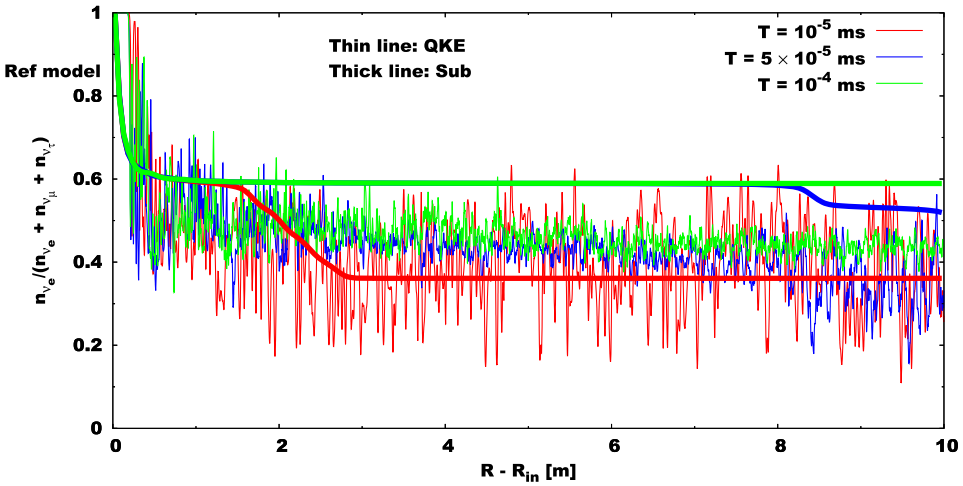

FIG. 2. The radial profile of angular-averaged survival probability of ν_e for the reference model. Different colors distinguish the results in the time snapshot from one another. The thin and thick lines show the results for the quantum kinetic simulation and the classical one with the BGK subgrid model, respectively.

the timescale of neutrino self-interactions at $R \gg R_{\rm in}$, indicating that ELN-XLN angular crossings almost disappear.

Although the overall properties can be well captured with the BGK subgrid model, there are quantitative deviations, the origins of which are worthy of discussion. In the early phase, the growth of flavor conversion is slightly faster for the classical simulation with the BGK subgrid model. This error comes from the empirical determination of τ_a via Eq. (17), which does not have the ability to determine the growth rate of FFC quantitatively. We also find that some detailed angular-dependent features are not captured by the subgrid model. In quantum kinetic simulations, flavor conversions vividly occur in the region of $0 \leq \cos\theta_\nu \lesssim 0.6$, but the angular region is slightly narrower for the subgrid model ($0 \leq \cos\theta_\nu \lesssim 0.5$). This is due mainly to the accuracy of the determination of η in our subgrid model. As described in Eqs. (29) and (30), the angular distribution of η is discrete at $G_\nu = 0$ in our approximate scheme, but it is continuous in the real scheme. Regarding this issue, one can reduce the error if we employ smooth functions to determine the angular distributions of η, although the numerical cost may become more expensive. We note that such approximate schemes were recently proposed by Xiong *et al.* [27], who showed that quadratic functions can reduce the error by 30% to 50% from our boxlike treatment.

In Figs. 4–6, we show the same plots as in Fig. 1 but for different models. These figures exhibit that the BGK subgrid model works well in all cases. One may think

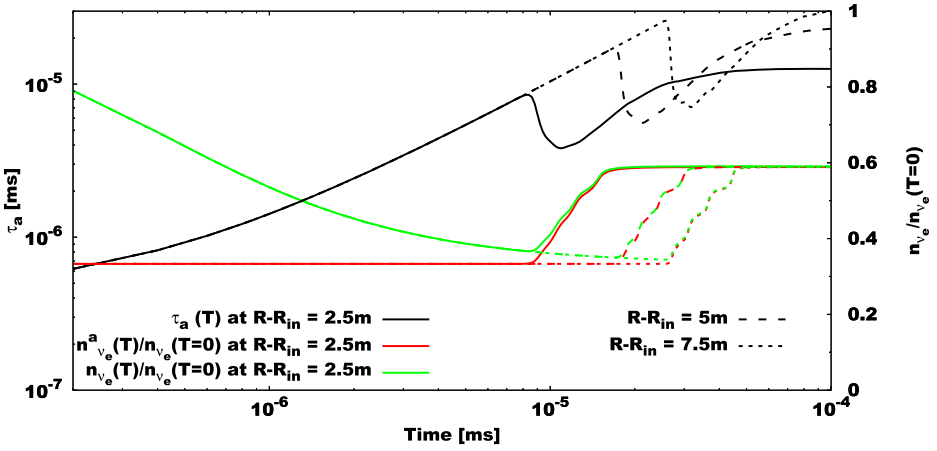

FIG. 3. Time evolution of τ_a (black lines), $n^a_{\nu_e}$ (red lines), and n_{ν_e} (green lines) at three spatial positions for the reference model. The line types distinguish the spatial positions from each other: $R - R_{\rm in} = 2.5$ m (solid lines), 5 m (dashed lines), and 7.5 m (dotted lines). The left and right y axes are for τ_a and $n^a_{\nu_e}$ (n_{ν_e}), respectively. In this plot, $n^a_{\nu_e}$ and n_{ν_e} are normalized by n_{ν_e} at $T = 0$ ms. See the text for more details.

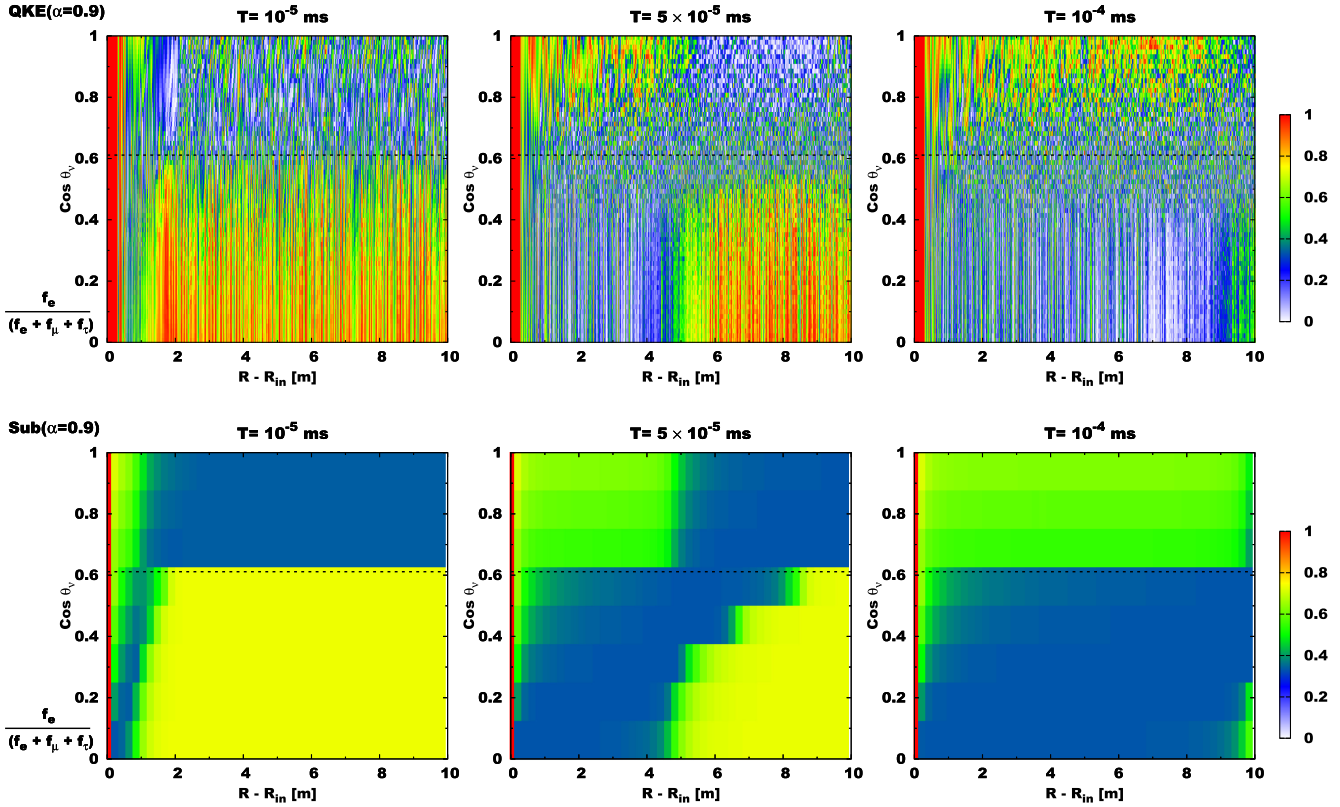

FIG. 4. Same as Fig. 1, but for the model with $\alpha = 0.9$ (and $\bar{\beta}_{ee} = 1$).

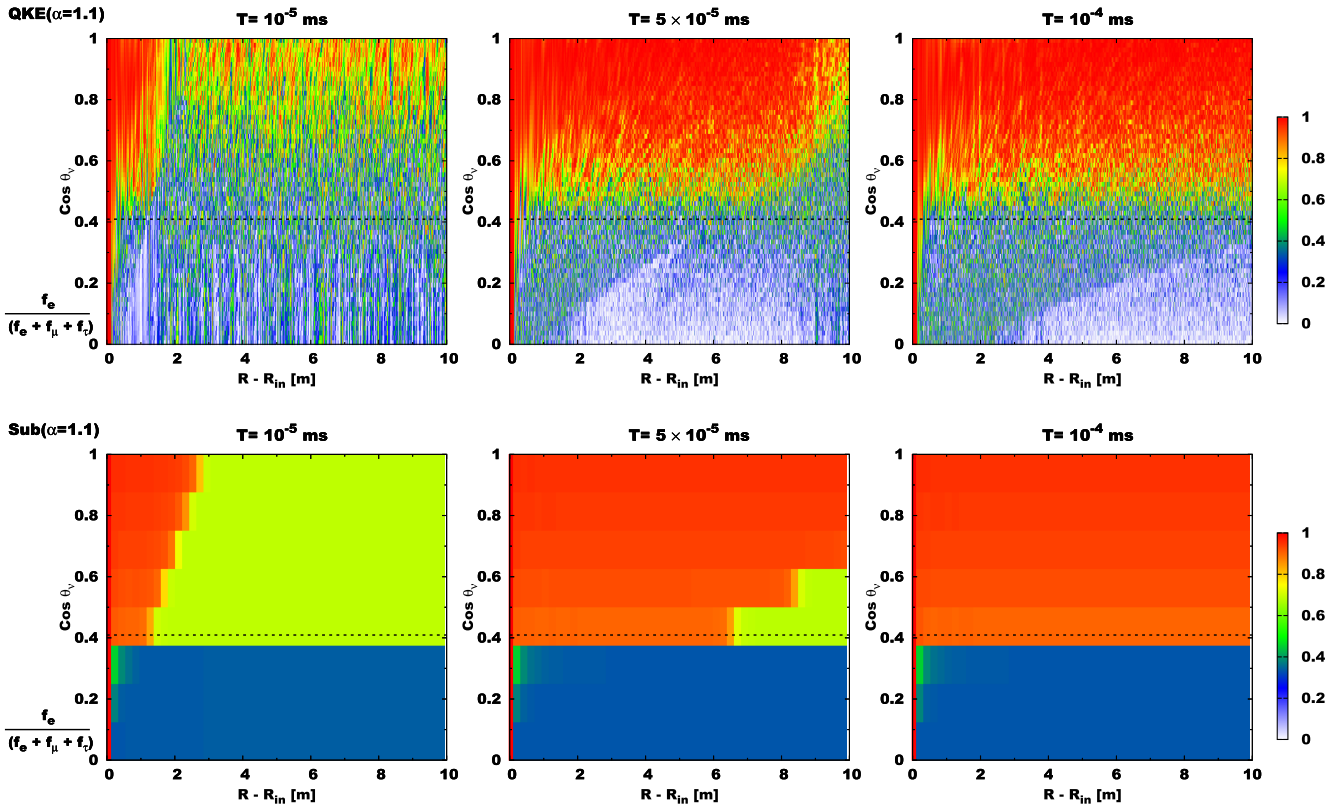

FIG. 5. Same as Fig. 1, but for the model with $\alpha = 1.1$ (and $\bar{\beta}_{ee} = 1$).

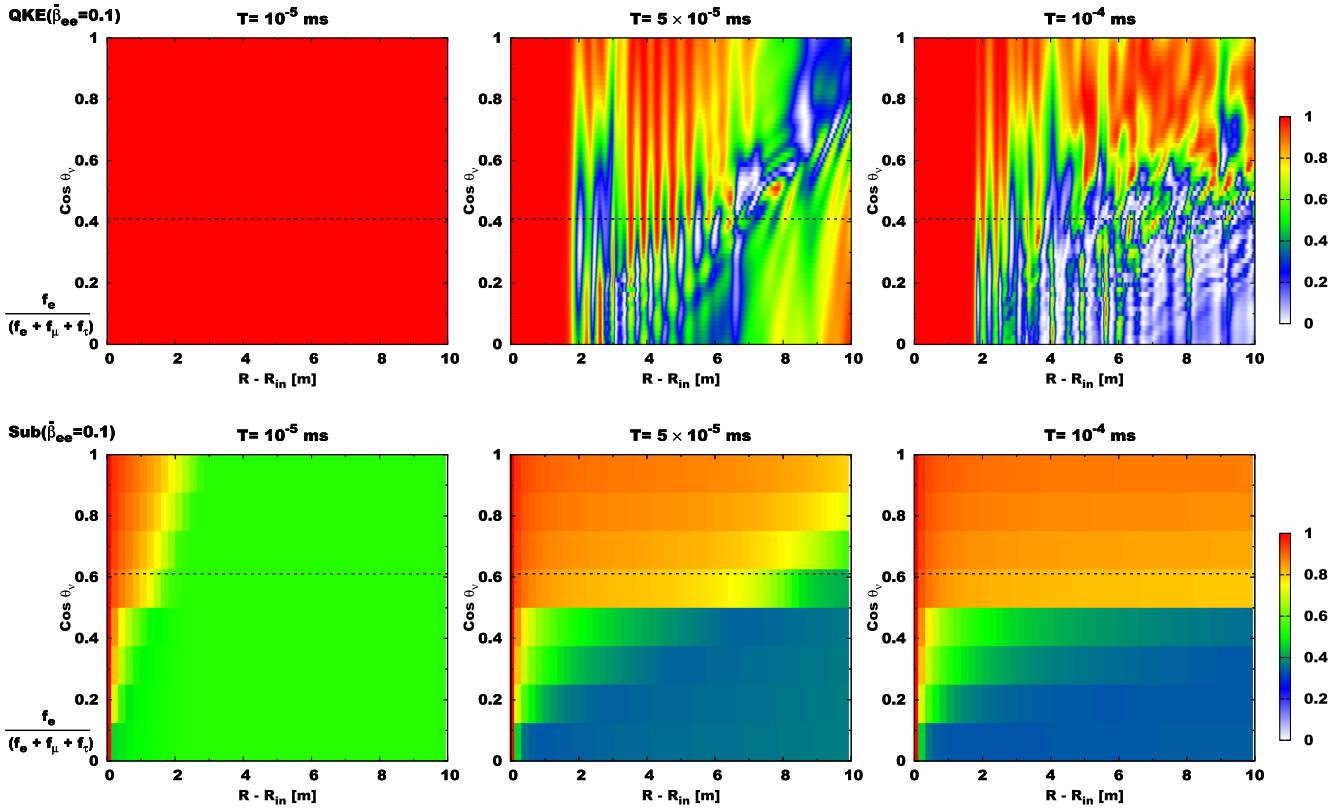

FIG. 6. Same as Fig. 1, but for the model with $\bar{\beta}_{ee} = 0.1$ (and $\alpha = 1.0$).

that the error around the boundary of $R - R_{\rm in} = 0$ in the model with $\bar{\beta}_{ee} = 0.1$ is higher than that in the other models. However, this error is also due to the low accuracy of determining τ_a. It can be improved if we employ better methods to determine it, for instance, those based on linear stability analysis. In Fig. 7, we compare the angular-averaged survival probabilities of ν_e at the end of our simulations from different models. For all models, we confirm that the error is within ∼20% for the asymptotic distribution of the neutrinos.

We show the result of our resolution study in Figs. 8 and 9, which correspond to the plot in Fig. 1. As can be seen in these figures, the overall features are essentially the same as the reference model, which leads to confidence that the BGK subgrid model is applicable to numerical simulations with coarse resolutions.

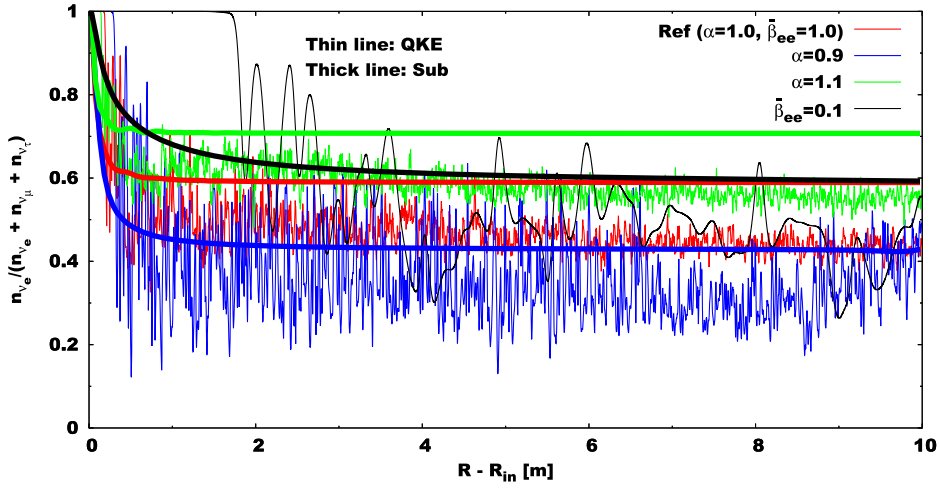

FIG. 7. Same as Fig. 2, but for all models. Different colors distinguish the various models. We display the results only at the end of simulation ($T = 10^{-4}$ ms).

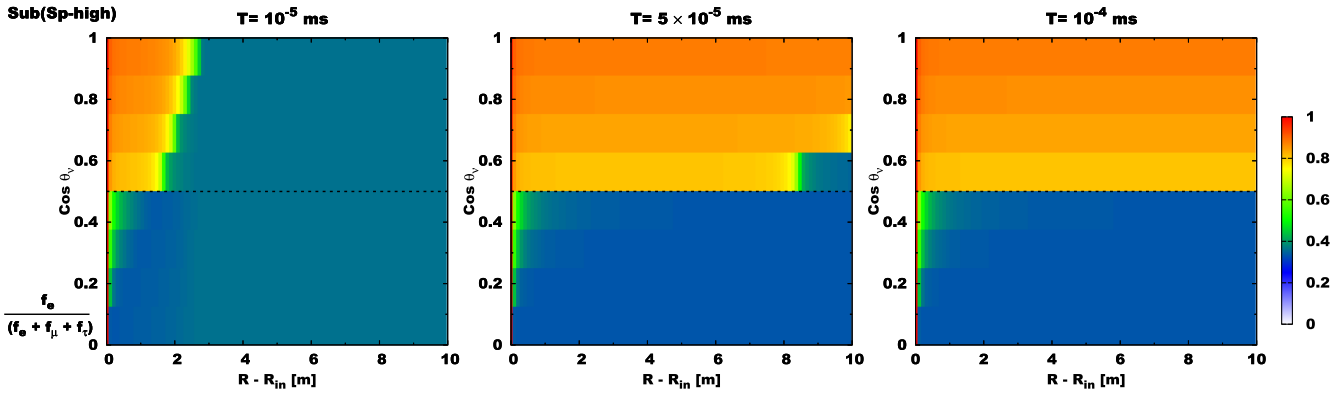

FIG. 8. Same as Fig. 1, but for a subgrid model (reference model) with twice the spatial resolution ($N_r = 384$) of the reference one.

Finally, we describe the reason why our BGK subgrid model with a prescription of Eqs. (28)–(30) works well, despite the fact that the flavor conversions in cases with the Dirichlet boundary are qualitatively different than the periodic one. We start by discussing the mechanism of transition of asymptotic states from the periodic case to the Dirichlet one. As shown above, we observed at least temporarily in the early nonlinear FFC phases that the asymptotic states determined from the number conservation (i.e., the periodic boundary case) appear in almost the entire spatial region. This is because the dynamics of flavor conversions is almost identical in the adjacent spatial regions, which offers an environment that is similar to a periodic boundary condition. As a result, the neutrino flux is also constant in adjacent spatial positions, guaranteeing the ELN and XLN conservation at each spatial position. On the other hand, both ELN and XLN fluxes (or first angular moments) in this (temporal) asymptotic state become different from those in initial conditions, whereas they are fixed in time at the boundary of $R = R_{\rm in}$ due to the Dirichlet condition. This is a crucial problem for asymptotic states since the number flux needs to be balanced to achieve the steady state [see Eq. (6) in [26]]. This implies that the neutrino distributions in the periodic boundary condition does not satisfy the actual asymptotic state. This also exhibits that ELN and XLN fluxes at $R > R_{\rm in}$ is different than $R = R_{\rm in}$, resulting in evolving ELN and XLN densities (or zeroth angular moments) at each spatial position.

One thing we notice along this discussion is that the classical simulation with BGK subgrid model has the ability to handle the effects of neutrino advection precisely since the advection term is the same as that in the quantum kinetic one. This indicates that the dynamical evolution of ELN and XLN densities at all spatial positions are well modeled. This also suggests that the neutrino radiation field obtained in the subgrid model evolves in time such that neutrino fluxes become constant in space to achieve the steady state, while this results in the dynamical change of ELN and XLN densities. In the BGK subgrid model, we determine f^a by the time- and spatial-dependent f to satisfy ELN and XLN densities at each position, which eventually leads to the consistent asymptotic state determined from the conservation of ELN and XLN fluxes. This corresponds to the asymptotic state with the Dirichlet boundary condition.

The above argument exhibits that the local study of flavor conversions with periodic boundary conditions is worthy of improving the BGK subgrid model. As demonstrated in [11,22,23,91], the global advection of neutrinos affects the dynamics of flavor conversion significantly, and

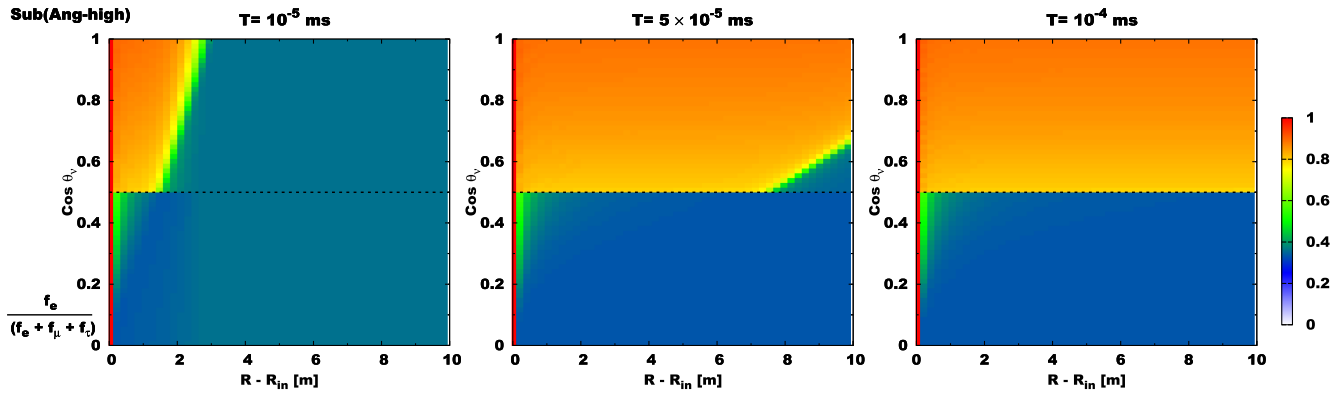

FIG. 9. Same as Fig. 1, but for a subgrid model (reference model) with higher angular resolution ($N_{\theta_\nu} = 128$) than the reference one.

the final outcome of neutrino radiation fields are qualitatively different than those estimated from local simulations. This study suggests, however, that the effects of global advection can be decoupled from local dynamics of flavor conversion under the framework of our BGK subgrid model. This suggests that the classical BGK model has the capability of modeling global quantum kinetics of neutrinos in CCSN and BNSM environments by precise determinations of f^a and τ_a based on a local study of flavor conversions.

VIII. SUMMARY

In this paper, we present a new subgrid model for neutrino quantum kinetics, particularly for neutrino-flavor conversion. The basic assumption in this subgrid model is to handle the dynamics of flavor conversions as a relaxation process in which the flavor conversion makes the system into asymptotic states (f^a) in the timescale of τ_a. This treatment is essentially the same as a BGK relaxation-time approximation [42], which was originally developed to approximately handle collisional processes in gas dynamics. In our model, we apply not the approximation to the collision term but instead the neutrino oscillation term. We describe the QKE with the BGK model in Sec. II and also provide an explicit form of the two-moment method in Sec. III. We also present a concrete example of how we can use the BGK model in classical neutrino transport by focusing on FFC (Sec. VII). We assess the capabilities of the BGK subgrid model by comparing it to the results of quantum kinetic neutrino transport, and we show that the subgrid model has the ability to capture the overall features in the dynamics of neutrino-flavor conversions.

Although our subgrid model is a valuable tool with great potential, more work is certainly needed to increase its accuracy. It should be pointed out that this study also provides a strategy to improve the subgrid model. As shown in Eq. (7), an accurate determination of η (and $\bar{\eta}$) from f is crucial, and all approaches, including analytic schemes [24–27] and AI [28], are applicable. We note that the prescription used in this demonstration [see Eqs. (28)–(30)] is just one example of FFC, and we certainly need others for different types of flavor conversions. In fact, the analytical scheme involving Eqs. (28)–(30) cannot handle the flavor swap phenomena recently found in FFC simulations of BNSM environments [22,34]. As such, we still need to improve approximate schemes to determine asymptotic states of FFCs.

We are also interested in how well the BGK subgrid model can work in cases in which flavor conversions and collision processes (neutrino emission, absorption, and scatterings) interact with each other. As demonstrated in [92–98], the asymptotic states of flavor conversion depend on neutrino-matter interactions. Detailed study is necessary to assess the capability of our subgrid model in such complicated systems. This detailed study is postponed to future work.

Although there is certainly room for improvement, the BGK subgrid model is very useful and easy to be implemented into currently existing CCSN and BNSM codes. This indicates that the global neutrino-radiation-hydrodynamic simulations with respectable physical fidelity of flavor conversions become feasible. We hope that the BGK subgrid model will contribute to the entire CCSN and BNSM community to incorporate the effects of neutrino quantum kinetics in their simulations.

ACKNOWLEDGMENTS

We are grateful to David Radice for the useful discussions. The numerical simulations were carried out using "Fugaku" and the high-performance computing resources of "Flow" at Nagoya University ICTS through the HPCI System Research Project (Projects No. 220173, No. 220047, No. 220223, No. 230033, No. 230204, and No. 230270), XC50 of CfCA at the National Astronomical Observatory of Japan (NAOJ), and Yukawa-21 at the Yukawa Institute for Theoretical Physics of Kyoto University. For providing high-performance computing resources, Computing Research Center, KEK, and JLDG on SINET of NII are acknowledged. This work is also supported by the High Energy Accelerator Research Organization (KEK). H. N. is supported by a Grant-in-Aid for Scientific Research (Grant No. 23K03468) and also by the NINS International Research Exchange Support Program. L. J. is supported by a Feynman Fellowship through LANL LDRD Project No. 20230788PRD1. M. Z. is supported by a JSPS Grant-in-Aid for JSPS Fellows (Grant No. 22KJ2906) from the Ministry of Education, Culture, Sports, Science, and Technology (MEXT) in Japan.

[1] Huaiyu Duan, George M. Fuller, and Yong-Zhong Qian, Collective neutrino oscillations, Annu. Rev. Nucl. Part. Sci. **60**, 569 (2010).

[2] Irene Tamborra and Shashank Shalgar, New developments in flavor evolution of a dense neutrino gas, Annu. Rev. Nucl. Part. Sci. **71**, 165 (2021).

[3] Sherwood Richers and Manibrata Sen, Fast flavor transformations, arXiv:2207.03561.

[4] Francesco Capozzi and Ninetta Saviano, Neutrino flavor conversions in high-density astrophysical and cosmological environments, Universe **8**, 94 (2022).

[5] Maria Cristina Volpe, Neutrinos from dense: Flavor mechanisms, theoretical approaches, observations, new directions, arXiv:2301.11814.

[6] Sajad Abbar, Francesco Capozzi, Robert Glas, H. Thomas Janka, and Irene Tamborra, On the characteristics of fast neutrino flavor instabilities in three-dimensional core-collapse supernova models, Phys. Rev. D **103**, 063033 (2021).

[7] Hiroki Nagakura, Adam Burrows, Lucas Johns, and George M. Fuller, Where, when, and why: Occurrence of fast-pairwise collective neutrino oscillation in three-dimensional core-collapse supernova models, Phys. Rev. D **104**, 083025 (2021).

[8] Ryuichiro Akaho, Jiabao Liu, Hiroki Nagakura, Masamichi Zaizen, and Shoichi Yamada, Collisional and fast neutrino flavor instabilities in two-dimensional core-collapse supernova simulation with Boltzmann neutrino transport, Phys. Rev. D **109**, 023012 (2024).

[9] Meng-Ru Wu and Irene Tamborra, Fast neutrino conversions: Ubiquitous in compact binary merger remnants, Phys. Rev. D **95**, 103007 (2017).

[10] Zewei Xiong, Lucas Johns, Meng-Ru Wu, and Huaiyu Duan, Collisional flavor instability in dense neutrino gases, Phys. Rev. D **108**, 083002 (2023).

[11] Hiroki Nagakura, Roles of fast neutrino-flavor conversion on the neutrino-heating mechanism of core-collapse supernova, Phys. Rev. Lett. **130**, 211401 (2023).

[12] Jakob Ehring, Sajad Abbar, Hans-Thomas Janka, Georg Raffelt, and Irene Tamborra, Fast neutrino flavor conversion in core-collapse supernovae: A parametric study in 1D models, Phys. Rev. D **107**, 103034 (2023).

[13] Jakob Ehring, Sajad Abbar, Hans-Thomas Janka, Georg Raffelt, and Irene Tamborra, Fast neutrino flavor conversions can help and hinder neutrino-driven explosions, Phys. Rev. Lett. **131**, 061401 (2023).

[14] Zewei Xiong, Andre Sieverding, Manibrata Sen, and Yong-Zhong Qian, Potential impact of fast flavor oscillations on neutrino-driven winds and their nucleosynthesis, Astrophys. J. **900**, 144 (2020).

[15] Manu George, Meng-Ru Wu, Irene Tamborra, Ricard Ardevol-Pulpillo, and Hans-Thomas Janka, Fast neutrino flavor conversion, ejecta properties, and nucleosynthesis in newly-formed hypermassive remnants of neutron-star mergers, Phys. Rev. D **102**, 103015 (2020).

[16] Xinyu Li and Daniel M. Siegel, Neutrino fast flavor conversions in neutron-star postmerger accretion disks, Phys. Rev. Lett. **126**, 251101 (2021).

[17] Rodrigo Fernández, Sherwood Richers, Nicole Mulyk, and Steven Fahlman, Fast flavor instability in hypermassive neutron star disk outflows, Phys. Rev. D **106**, 103003 (2022).

[18] Oliver Just, Sajad Abbar, Meng-Ru Wu, Irene Tamborra, Hans-Thomas Janka, and Francesco Capozzi, Fast neutrino conversion in hydrodynamic simulations of neutrino-cooled accretion disks, Phys. Rev. D **105**, 083024 (2022).

[19] Shin-ichiro Fujimoto and Hiroki Nagakura, Explosive nucleosynthesis with fast neutrino-flavour conversion in core-collapse supernovae, Mon. Not. R. Astron. Soc. **519**, 2623 (2023).

[20] Hiroki Nagakura and Masamichi Zaizen, Time-dependent and quasisteady features of fast neutrino-flavor conversion, Phys. Rev. Lett. **129**, 261101 (2022).

[21] Zewei Xiong, Meng-Ru Wu, Gabriel Martínez-Pinedo, Tobias Fischer, Manu George, Chun-Yu Lin, and Lucas Johns, Evolution of collisional neutrino flavor instabilities in spherically symmetric supernova models, Phys. Rev. D **107**, 083016 (2023).

[22] Hiroki Nagakura, Global features of fast neutrino-flavor conversion in binary neutron star mergers, Phys. Rev. D **108**, 103014 (2023).

[23] Shashank Shalgar and Irene Tamborra, Neutrino flavor conversion, advection, and collisions: Toward the full solution, Phys. Rev. D **107**, 063025 (2023).

[24] Hiroki Nagakura and Masamichi Zaizen, Connecting small-scale to large-scale structures of fast neutrino-flavor conversion, Phys. Rev. D **107**, 063033 (2023).

[25] Masamichi Zaizen and Hiroki Nagakura, Simple method for determining asymptotic states of fast neutrino-flavor conversion, Phys. Rev. D **107**, 103022 (2023).

[26] Masamichi Zaizen and Hiroki Nagakura, Characterizing quasisteady states of fast neutrino-flavor conversion by stability and conservation laws, Phys. Rev. D **107**, 123021 (2023).

[27] Zewei Xiong, Meng-Ru Wu, Sajad Abbar, Soumya Bhattacharyya, Manu George, and Chun-Yu Lin, Evaluating approximate asymptotic distributions for fast neutrino flavor conversions in a periodic 1D box, Phys. Rev. D **108**, 063003 (2023).

[28] Sajad Abbar, Meng-Ru Wu, and Zewei Xiong, Physics-informed neural networks for predicting the asymptotic outcome of fast neutrino flavor conversions, Phys. Rev. D **109**, 043024 (2024).

[29] Lucas Johns, Thermodynamics of oscillating neutrinos, arXiv:2306.14982.

[30] Meng-Ru Wu, Manu George, Chun-Yu Lin, and Zewei Xiong, Collective fast neutrino flavor conversions in a 1D box: Initial conditions and long-term evolution, Phys. Rev. D **104**, 103003 (2021).

[31] Sherwood Richers, Donald Willcox, and Nicole Ford, Neutrino fast flavor instability in three dimensions, Phys. Rev. D **104**, 103023 (2021).

[32] Soumya Bhattacharyya and Basudeb Dasgupta, Elaborating the ultimate fate of fast collective neutrino flavor oscillations, Phys. Rev. D **106**, 103039 (2022).

[33] Sherwood Richers, Huaiyu Duan, Meng-Ru Wu, Soumya Bhattacharyya, Masamichi Zaizen, Manu George, Chun-Yu Lin, and Zewei Xiong, Code comparison for fast flavor instability simulations, Phys. Rev. D **106**, 043011 (2022).

[34] Masamichi Zaizen and Hiroki Nagakura, Fast neutrino-flavor swap in high-energy astrophysical environments, arXiv:2311.13842.
[35] Steen Hannestad, Georg G. Raffelt, Günter Sigl, and Yvonne Y. Y. Wong, Self-induced conversion in dense neutrino gases: Pendulum in flavor space, Phys. Rev. D **74**, 105010 (2006).
[36] Lucas Johns, Hiroki Nagakura, George M. Fuller, and Adam Burrows, Neutrino oscillations in supernovae: Angular moments and fast instabilities, Phys. Rev. D **101**, 043009 (2020).
[37] Ian Padilla-Gay, Irene Tamborra, and Georg G. Raffelt, Neutrino flavor pendulum reloaded: The case of fast pairwise conversion, Phys. Rev. Lett. **128**, 121102 (2022).
[38] Damiano F. G. Fiorillo and Georg G. Raffelt, Flavor solitons in dense neutrino gases, Phys. Rev. D **107**, 123024 (2023).
[39] Lucas Johns and Santiago Rodriguez, Collisional flavor pendula and neutrino quantum thermodynamics, arXiv:2312.10340.
[40] Damiano F. G. Fiorillo and Georg G. Raffelt, Slow and fast collective neutrino oscillations: Invariants and reciprocity, Phys. Rev. D **107**, 043024 (2023).
[41] Damiano F. G. Fiorillo, Ian Padilla-Gay, and Georg G. Raffelt, Collisions and collective flavor conversion: Integrating out the fast dynamics, arXiv:2312.07612.
[42] P. L. Bhatnagar, E. P. Gross, and M. Krook, A model for collision processes in gases. I. Small amplitude processes in charged and neutral one-component systems, Phys. Rev. **94**, 511 (1954).
[43] Hiroki Nagakura, General-relativistic quantum-kinetics neutrino transport, Phys. Rev. D **106**, 063011 (2022).
[44] Lucas Johns, Ergodicity demystifies fast neutrino flavor instability, arXiv:2402.08896.
[45] Lucas Johns, Derivation of the sterile neutrino Boltzmann equation from quantum kinetics, Phys. Rev. D **100**, 083536 (2019).
[46] H. Nagakura, W. Iwakami, S. Furusawa, K. Sumiyoshi, S. Yamada, H. Matsufuru, and A. Imakura, Three-dimensional Boltzmann-hydro code for core-collapse in massive stars. II. The implementation of moving-mesh for neutron star kicks, Astrophys. J. Suppl. Ser. **229**, 42 (2017).
[47] M. Shibata, H. Nagakura, Y. Sekiguchi, and S. Yamada, Conservative form of Boltzmann's equation in general relativity, Phys. Rev. D **89**, 084073 (2014).
[48] K. Sumiyoshi and S. Yamada, Neutrino transfer in three dimensions for core-collapse supernovae. I. Static configurations, Astrophys. J. Suppl. Ser. **199**, 17 (2012).
[49] H. Nagakura, K. Sumiyoshi, and S. Yamada, Three-dimensional Boltzmann hydro code for core collapse in massive stars. I. Special relativistic treatments, Astrophys. J. Suppl. Ser. **214**, 16 (2014).
[50] Amol S. Dighe and Alexei Yu. Smirnov, Identifying the neutrino mass spectrum from a supernova neutrino burst, Phys. Rev. D **62**, 033007 (2000).
[51] Hiroki Nagakura, Adam Burrows, David Vartanyan, and David Radice, Core-collapse supernova neutrino emission and detection informed by state-of-the-art three-dimensional numerical models, Mon. Not. R. Astron. Soc. **500**, 696 (2021).
[52] Hiroki Nagakura, Retrieval of energy spectra for all flavours of neutrinos from core-collapse supernova with multiple detectors, Mon. Not. R. Astron. Soc. **500**, 319 (2021).
[53] Hiroki Nagakura and Kenta Hotokezaka, Non-thermal neutrinos created by shock acceleration in successful and failed core-collapse supernova, Mon. Not. R. Astron. Soc. **502**, 89 (2021).
[54] C. J. Horowitz, Weak magnetism for antineutrinos in supernovae, Phys. Rev. D **65**, 043001 (2002).
[55] R. Bollig, H. T. Janka, A. Lohs, G. Martínez-Pinedo, C. J. Horowitz, and T. Melson, Muon creation in supernova matter facilitates neutrino-driven explosions, Phys. Rev. Lett. **119**, 242702 (2017).
[56] Tobias Fischer, Gang Guo, Gabriel Martínez-Pinedo, Matthias Liebendörfer, and Anthony Mezzacappa, Muonization of supernova matter, Phys. Rev. D **102**, 123001 (2020).
[57] Gang Guo, Gabriel Martínez-Pinedo, A. Lohs, and Tobias Fischer, Charged-current muonic reactions in core-collapse supernovae, Phys. Rev. D **102**, 023037 (2020).
[58] M. Shibata, K. Kiuchi, Y. Sekiguchi, and Y. Suwa, Truncated moment formalism for radiation hydrodynamics in numerical relativity, Prog. Theor. Phys. **125**, 1255 (2011).
[59] C. Y. Cardall, E. Endeve, and A. Mezzacappa, Conservative $3+1$ general relativistic variable Eddington tensor radiation transport equations, Phys. Rev. D **87**, 103004 (2013).
[60] Francois Foucart, Evan O'Connor, Luke Roberts, Matthew D. Duez, Roland Haas, Lawrence E. Kidder, Christian D. Ott, Harald P. Pfeiffer, Mark A. Scheel, and Bela Szilagyi, Post-merger evolution of a neutron star-black hole binary with neutrino transport, Phys. Rev. D **91**, 124021 (2015).
[61] O. Just, M. Obergaulinger, and H. T. Janka, A new multi-dimensional, energy-dependent two-moment transport code for neutrino-hydrodynamics, Mon. Not. R. Astron. Soc. **453**, 3386 (2015).
[62] T. Kuroda, T. Takiwaki, and K. Kotake, A new multi-energy neutrino radiation-hydrodynamics code in full general relativity and its application to the gravitational collapse of massive stars, Astrophys. J. Suppl. Ser. **222**, 20 (2016).
[63] Evan P. O'Connor and Sean M. Couch, Two-dimensional core-collapse supernova explosions aided by general relativity with multidimensional neutrino transport, Astrophys. J. **854**, 63 (2018).
[64] M. Aaron Skinner, Joshua C. Dolence, Adam Burrows, David Radice, and David Vartanyan, FORNAX: A flexible code for multiphysics astrophysical simulations, Astrophys. J. Suppl. Ser. **241**, 7 (2019).
[65] Lukas R. Weih, Hector Olivares, and Luciano Rezzolla, Two-moment scheme for general-relativistic radiation hydrodynamics: A systematic description and new applications, Mon. Not. R. Astron. Soc. **495**, 2285 (2020).
[66] Anthony Mezzacappa, Eirik Endeve, O. E. Bronson Messer, and Stephen W. Bruenn, Physical, numerical, and computational challenges of modeling neutrino transport in core-collapse supernovae, Living Rev. Comput. Astrophys. **6**, 4 (2020).
[67] M. Paul Laiu, Eirik Endeve, Ran Chu, J. Austin Harris, and O. E. Bronson Messer, A DG-IMEX method for two-moment neutrino transport: Nonlinear solvers for neutrino-matter coupling, Astrophys. J. Suppl. Ser. **253**, 52 (2021).

[68] David Radice, Sebastiano Bernuzzi, Albino Perego, and Roland Haas, A new moment-based general-relativistic neutrino-radiation transport code: Methods and first applications to neutron star mergers, Mon. Not. R. Astron. Soc. **512**, 1499 (2022).
[69] Patrick Chi-Kit Cheong, Harry Ho-Yin Ng, Alan Tsz-Lok Lam, and Tjonnie Guang Feng Li, General-relativistic radiation transport scheme in GMUNU. I. Implementation of two-moment-based multifrequency radiative transfer and code tests, Astrophys. J. Suppl. Ser. **267**, 38 (2023).
[70] Lucas Johns, Hiroki Nagakura, George M. Fuller, and Adam Burrows, Fast oscillations, collisionless relaxation, and spurious evolution of supernova neutrino flavor, Phys. Rev. D **102**, 103017 (2020).
[71] McKenzie Myers, Theo Cooper, MacKenzie Warren, Jim Kneller, Gail McLaughlin, Sherwood Richers, Evan Grohs, and Carla Fröhlich, Neutrino flavor mixing with moments, Phys. Rev. D **105**, 123036 (2022).
[72] Evan Grohs, Sherwood Richers, Sean M. Couch, Francois Foucart, James P. Kneller, and G. C. McLaughlin, Neutrino fast flavor instability in three dimensions for a neutron star merger, Phys. Lett. B **846**, 138210 (2023).
[73] Julien Froustey, Sherwood Richers, Evan Grohs, Samuel Flynn, Francois Foucart, James P. Kneller, and Gail C. McLaughlin, Neutrino fast flavor oscillations with moments: Linear stability analysis and application to neutron star mergers, Phys. Rev. D **109**, 043046 (2024).
[74] K. S. Thorne, Relativistic radiative transfer—Moment formalisms, Mon. Not. R. Astron. Soc. **194**, 439 (1981).
[75] Lucas Johns and Hiroki Nagakura, Fast flavor instabilities and the search for neutrino angular crossings, Phys. Rev. D **103**, 123012 (2021).
[76] Sherwood Richers, Evaluating approximate flavor instability metrics in neutron star mergers, Phys. Rev. D **106**, 083005 (2022).
[77] Hiroki Nagakura and Lucas Johns, Constructing angular distributions of neutrinos in core-collapse supernovae from zeroth and first moments calibrated by full Boltzmann neutrino transport, Phys. Rev. D **103**, 123025 (2021).
[78] Jiabao Liu, Ryuichiro Akaho, Akira Ito, Hiroki Nagakura, Masamichi Zaizen, and Shoichi Yamada, Universality of the neutrino collisional flavor instability in core-collapse supernovae, Phys. Rev. D **108**, 123024 (2023).
[79] Jiabao Liu, Masamichi Zaizen, and Shoichi Yamada, Systematic study of the resonancelike structure in the collisional flavor instability of neutrinos, Phys. Rev. D **107**, 123011 (2023).
[80] Chinami Kato, Hiroki Nagakura, and Lucas Johns, Collisional flavor swap with neutrino self-interactions, arXiv: 2309.02619.
[81] Ignacio Izaguirre, Georg Raffelt, and Irene Tamborra, Fast pairwise conversion of supernova neutrinos: A dispersion relation approach, Phys. Rev. Lett. **118**, 021101 (2017).
[82] Sagar Airen, Francesco Capozzi, Sovan Chakraborty, Basudeb Dasgupta, Georg Raffelt, and Tobias Stirner, Normal-mode analysis for collective neutrino oscillations, J. Cosmol. Astropart. Phys. 12 (2018) 019.
[83] Hiroki Nagakura, Taiki Morinaga, Chinami Kato, and Shoichi Yamada, Fast-pairwise collective neutrino oscillations associated with asymmetric neutrino emissions in core-collapse supernovae, Astrophys. J. **886**, 139 (2019).
[84] Taiki Morinaga, Hiroki Nagakura, Chinami Kato, and Shoichi Yamada, Fast neutrino-flavor conversion in the preshock region of core-collapse supernovae, Phys. Rev. Res. **2**, 012046 (2020).
[85] Basudeb Dasgupta, Alessandro Mirizzi, and Manibrata Sen, Simple method of diagnosing fast flavor conversions of supernova neutrinos, Phys. Rev. D **98**, 103001 (2018).
[86] Sajad Abbar, Searching for fast neutrino flavor conversion modes in core-collapse supernova simulations, J. Cosmol. Astropart. Phys. 05 (2020) 027.
[87] Hiroki Nagakura and Lucas Johns, New method for detecting fast neutrino flavor conversions in core-collapse supernova models with two-moment neutrino transport, Phys. Rev. D **104**, 063014 (2021).
[88] Lucas Johns, Collisional flavor instabilities of supernova neutrinos, Phys. Rev. Lett. **130**, 191001 (2023).
[89] Sajad Abbar, Applications of machine learning to detecting fast neutrino flavor instabilities in core-collapse supernova and neutron star merger models, Phys. Rev. D **107**, 103006 (2023).
[90] Sajad Abbar and Hiroki Nagakura, Detecting fast neutrino flavor conversions with machine learning, Phys. Rev. D **109**, 023033 (2024).
[91] Hiroki Nagakura and Masamichi Zaizen, Basic characteristics of neutrino flavor conversions in the postshock regions of core-collapse supernova, Phys. Rev. D **108**, 123003 (2023).
[92] Shashank Shalgar and Irene Tamborra, Change of direction in pairwise neutrino conversion physics: The effect of collisions, Phys. Rev. D **103**, 063002 (2021).
[93] Joshua D. Martin, J. Carlson, Vincenzo Cirigliano, and Huaiyu Duan, Fast flavor oscillations in dense neutrino media with collisions, Phys. Rev. D **103**, 063001 (2021).
[94] Hirokazu Sasaki and Tomoya Takiwaki, A detailed analysis of the dynamics of fast neutrino flavor conversions with scattering effects, Prog. Theor. Exp. Phys. **2022**, 073E01 (2022).
[95] Chinami Kato and Hiroki Nagakura, Effects of energy-dependent scatterings on fast neutrino flavor conversions, Phys. Rev. D **106**, 123013 (2022).
[96] Günter Sigl, Simulations of fast neutrino flavor conversions with interactions in inhomogeneous media, Phys. Rev. D **105**, 043005 (2022).
[97] Ian Padilla-Gay, Irene Tamborra, and Georg G. Raffelt, Neutrino fast flavor pendulum. II. Collisional damping, Phys. Rev. D **106**, 103031 (2022).
[98] Chinami Kato, Hiroki Nagakura, and Masamichi Zaizen, Flavor conversions with energy-dependent neutrino emission and absorption, Phys. Rev. D **108**, 023006 (2023).